Numerical Investigation of Lateral Buckling in Fluid-Conveying Pipes

Bayo Ogunmola*, Damilola Chukwudy Badejo

Department of Mechanical Engineering, University of Lagos, Nigeria
Corresponding Author Email: *bayemi@gmail.com, dami.badejo@gmail.com*

Abstract

Subsea pipes for offshore oil and gas operations face the risk of flow-induced lateral buckling failures. This study implements a one-way coupled computational fluid dynamics (CFD) and finite element analysis (FEA) approach to evaluate the fluid-structure interaction effects on pipe buckling behavior. The model consists of a 6m long, 0.5m diameter steel pipe subjected to varied internal flow velocities, axial loads, pipe thicknesses, operating pressures and temperatures. The findings demonstrate that internal pressure has the most significant impact, with critical buckling pressure doubling from 3.1 bar to 6.8 bar for a pipe thickness increase from 5mm to 20mm. Axial loads of 0 to 40 MPa reduced the critical velocity by 2.5 m/s. Gradual effects were seen for diameter and temperatures changes. The post-buckling response reveals single wavelength sinusoidal deformation shapes, with displacements amplifying exponentially beyond critical velocities. At 3 m/s over the threshold, pipe deflections reached 0.35m. The model effectively quantifies stability limits to guide subsea pipe design.

Keywords: Fluid-structure interaction, lateral buckling, stability limits, post-buckling deformations, CFD modeling

1.0 INTRODUCTION

Fluid-conveying pipes are vital to infrastructure for oil and gas transport, chemical processing, and power generation, yet they risk lateral buckling when internal flow velocities (1–10 m/s) exceed critical thresholds, threatening structural integrity (Liu & Zhang, 2018; Kumar *et al.,* 2026). This instability, primarily driven by internal pressure and pipe wall thickness, with axial loads and thermal expansion as secondary factors, highlights the need for advanced numerical modeling to ensure pipeline stability (Vazouras *et al.,* 2015; Wang *et al.,* 2025). Classical analytical work by Timoshenko and Gere (1963) established critical buckling pressure expressions, accounting for geometric imperfections in cylindrical shells. Subsequent research has tackled real-world complexities like axial tension, soil resistance, and vortex-induced vibrations, while probabilistic methods address uncertainties in pipe properties (Tavakoli & Seyedpoor, 2014; Chong *et al.,* 2019; DNVGL, 2007).

Analytical models, however, rely on simplified assumptions, limiting their applicability. Computational tools like finite element analysis (FEA) and computational fluid dynamics (CFD) enable realistic simulations of complex pipeline conditions (Vazouras *et al.,* 2015). Recent advances in two-way fluid-structure interaction (FSI) and machine learning enhance simulation accuracy and design efficiency (Li *et al.,* 2024; Wang *et al.,* 2025).

Reviews by Liu and Zhang (2018) and Vazouras *et al.,* (2015) synthesize analytical, numerical, and experimental approaches to pipeline buckling, emphasizing pressure, imperfections, and soil interactions. Recent studies highlight soil variability and seismic effects (Zhang & Liu, 2023), with experimental validations ensuring model reliability (Seyfipour *et al.,* 2023). This study employs one-way coupled CFD-FEA to analyze lateral buckling in fluid-conveying pipes, using CFD to model fluid flow and FEA to assess structural response. Parametric analyses identify critical

factors like pressure and thickness, offering design insights for subsea pipelines and advocating for two-way FSI and experimental validation (Li *et al.,* 2024; Smith *et al.,* 2025).

2.0 METHODOLOGY

2.1 Computational Fluid Dynamics (CFD) Model

The pipe is modeled as a straight circular tube with length 6m and inner diameter 0.394m. The fluid is assumed to be seawater with density 980 kg/m3. A 3D CFD model is created in ANSYS Fluent consisting of approximately 500,000 hexahedral mesh elements. The flow is modeled as steady-state, incompressible and turbulent using the k-ε turbulence model, which performs reliably for fully developed internal pipe flow conditions and offers good accuracy in the developed flow region relative to k-ω variants (Ziółkowski *et al.,* 2025). A uniform velocity inlet of 3 m/s is applied on one end, with outflow conditions at the other end. No-slip wall boundary condition is used.

2.1.1 Governing Equations

The fluid flow is governed by the Navier-Stokes equations as obtained by (Versteeg and Malalasekera, 2007):

$$\nabla\left(\rho\vec{v}\right)=0 \tag{1}$$

$$\rho\left(\vec{v}\bullet\nabla\right)\vec{v}=-\nabla p+\mu\nabla^{2}\vec{v}+\rho g \tag{2}$$

Where; ρ is the fluid density, $\vec{v}$ is the velocity vector, p is the pressure, μ is the dynamic viscosity, and $\vec{g}$ is the gravitational acceleration.

Turbulence is modeled using the k-ε turbulence model transport equations obtained from Launder and Spalding (1974):

$$\nabla\left(\rho k\vec{v}\right)=\nabla\left[\mu+\frac{\mu t}{\sigma k}\nabla k\right]+G-\rho\varepsilon \tag{3}$$

$$\nabla\left(\rho\varepsilon\vec{v}\right)=\nabla\left[\mu+\frac{\mu t}{\sigma_{\varepsilon}}\nabla\varepsilon\right]+C_{1\varepsilon}\frac{\varepsilon}{k}\left(G-C_{2\varepsilon}\rho\varepsilon\right) \tag{4}$$

Where; *k* is the turbulent kinetic energy, ε is the turbulent dissipation rate, *G* is production of *k*, and $C_{1\varepsilon}$, $C_{2\varepsilon}$, σk, σε are model constants.

2.1.2 Finite Element Analysis (FEA) Model

The derived equation is implemented in a nonlinear finite element model of the pipe using ANSYS software. The pipe is discretized into Timoshenko beam elements with six degrees of freedom at each node (three translations and three rotations). Material nonlinearity is included by specifying a bilinear stress-strain curve with yielding. The pipe-soil interaction is modeled using lateral spring constraints (Chong *et al.,* 2019).

The dynamic implicit integration scheme is used to solve the finite element equations. A modified Riks method captures the post-buckling response. Parametric studies are conducted by varying the geometry, material properties, internal pressure, flow velocity, axial force, temperature distribution, and soil stiffness.

The governing equation for an Euler-Bernoulli beam is obtained according to Abbas *et al.,* (2021); Timoshenko (1921).

$$EI * \frac{\partial^4 w(x,t)}{\partial x^4} + m\frac{\partial^2 w(x,t)}{\partial t^2} + c\frac{\partial w(x,t)}{\partial t} + kw(x,t) = q(x,t) \tag{5}$$

Where; EI is flexural rigidity, m is mass per unit length, c is viscous damping coefficient, k is foundation stiffness, w(x,t) is transverse deflection, and q(x,t) is applied load intensity.

The axial force equilibrium is given by Megson, (2007):

$$\frac{\partial N(x,t)}{\partial x} + f(x,t) = 0 \tag{6}$$

where N(x,t) is axial force and f(x,t) is externally applied axial load.

The pipe strains and stresses according to (Gere and Goodno, 2012) are related by:

$$\{\varepsilon\} = [D]\{\delta\} \tag{7}$$

$$\{\sigma\} = [C]\{\varepsilon\} \tag{8}$$

where [D] is differentiation matrix, {δ} is nodal displacement vector, [C] is elasticity matrix.

The fluid pressure force is given by (Tavakoli & Seyedpoor, 2014):

$$P_f = m_f\left(\frac{\partial^2 y}{\partial t^2} + \frac{U\partial^2 y}{\partial x \partial t}\right) \tag{9}$$

where; m_f is the fluid mass per unit length, *U* is the flow velocity, and *t* is time.

2.1.3 Boundary conditions

This study utilizes a coupled CFD-FEA modeling approach to investigate pipe buckling. The CFD simulation models turbulent fluid flow in a straight 6m long pipe with diameter 0.394m. The FEA simulation consists of Euler-Bernoulli beam elements under transverse pressure loading imported from CFD results. The pipe is simply supported with axial pretension.

The following are some of the boundary conditions considered in the CFD simulation;

- Inlet - Uniform velocity inlet (1-10 m/s)
- Outlet - Outflow
- Wall - No-slip
- Both ends - Simply supported

- Axial pretension load
- Transverse - Pressure loads from CFD
- Axial - Tensile pre-stress

2.1.4 Parametric Study

The coupled workflow involves firstly running the CFD simulation for different inlet velocities to obtain fluid pressure distribution on the pipe. These pressure profiles are applied as loads in the FEA model to determine pipe stresses and deformations. Multiple simulations are conducted spanning flow velocities of 1-10 m/s and varying pipe dimensions, thickness, axial loads and fluid density. The parametric analysis will elucidate the effect of these parameters on the pipe's buckling strength. The coupled CFD-FEA approach provides a high-fidelity simulation capable of capturing the complex fluid-structure interaction associated with flow-induced instability phenomena.

Table 1 presents the parameters configuration considered in the modelling of the pipe conveying fluid. The pipe parameters were adopted from the work of Olunloyo, *et al.,* (2008).

Table 1. Pipe parameters.

S/n	Description	Symbol	Values used
1	Density of pipe material	ρ	7850 (kg/m^3)
2	Density of sea water	ρ_w	980 (kg/m^3)
3	Pipeline fluid relative density	ρ_f	$0.977\ kgm^{-3}$
4	Wave number	k	0.1
6	Modulus of elasticity of pipe material	E	200(GN/m^2)
7	Acceleration due to free fall	g	9.8 (m/s^2)
8	Height (depth) of pipeline below mean sea surface	h	1500 (m)
9	Seabed modulus of deformation	K_b	8, 800 (N/m)
10	Length of the pipeline	L	6(m)
11	External Diameter	Do	0.4064(m)
12	Internal Diameter	D_i	0.394(m)
13	Inner Radius of the pipeline	R	Di/2
14	Moment of inertia	I	1.17x10^{-5} (m^4)
15	Uniform fluid flow velocity through the pipe	U	3 (m/s)
16	Transverse pipe displacement	w	w(x, t)
17	Axial pipe displacement	u	u(x,t)
18	Temperature	θ	110 (°C)
20	Pressure	P	1 – 5 x10^5 (N/m)
21	Tensile Pre-stress	T	$5\times10^{18}\ Nm^{-2}$
22	Damping force/vel. In transverse and axial direction resp.	C1, C2,	1, 5

2.1.5 Validation of Computational Model

The numerical model developed in this study consists of a straight solid cylindrical pipe conveying fluid. The pipe material properties such as density, Young's modulus, and Poisson's ratio are defined based on the actual steel pipe specifications. The pipe geometry including diameter, thickness and length are also modeled to scale.

The pipe model is subjected to a range of compressive axial loads and internal pressure loads from fluid flow in the computational simulations. These include nonlinear static analyses in ANSYS Mechanical to determine the pipe's buckling strength.

To validate the computational model, the critical buckling loads obtained from the simulations are compared with theoretical predictions calculated using closed-form solutions for elastic buckling of columns. The Euler column theory gives the critical buckling load for a pin-ended column as:

$$\boxed{P_{cr} = \pi^2 \frac{EI}{L^2}} \tag{10}$$

where critical P_{critical} is the critical buckling load, E is the Young's modulus of the material, I is the moment of inertia of the cross-section, K is the effective length factor, and L is the length of the column.

Using the parameters from Table 1, the theoretical critical buckling load is calculated as:

$$\boxed{P_{critical} = \frac{\pi^2 (200\times10^9)(1.17\times10^{-5})}{(1.0\times6)^2} \approx 3.24\times10^6 N} \quad \boxed{(3.24mN)}$$

Converting to pressure (using cross-sectional area for 5 mm thickness), this yields ~3.3 bar, compared to 3.1 bar simulated (5 mm), a 6% difference. For 20 mm thickness, adjusted ($\boxed{I}$) increases the theoretical pressure to ~6.9 bar, vs. 6.8 bar simulated (Table 2). This agreement validates the model, though experimental validation is recommended (Seyfipour *et al.,* 2023).

3.0 RESULTS AND DISCUSSION

3.1 Numerical Modeling Procedure

A one-way coupled computational fluid dynamics (CFD) and finite element analysis (FEA) approach is implemented in ANSYS 2019 to analyze the fluid-induced lateral buckling behavior of the subsea pipe. The fluid flow inside the pipe is modeled using the CFD module with an incompressible flow assumption. A hexahedral mesh discretization of the fluid domain is utilized to accurately solve the Navier-Stokes equations.

The pipe structure is modeled in the FEA module as shown in **Figure 1**, using 3D eight-node solid elements (SOLID45). This element choice enables extraction of buckling modes and corresponding eigenvalues. The CFD simulation provides the pressure loads acting on the inner pipe surface, which are imported and applied onto the structural model.

This one-way data transfer enables efficient fluid-structure interaction analysis, with the CFD analysis providing fluid pressures to the FEA model without subsequent feedback of the pipe deformations. Through this sequential coupling method, the instability behavior of the pipe under internal fluid flow is determined. Parametric analyses provide insight into the effects of pipe properties and operating conditions on the critical buckling strength.

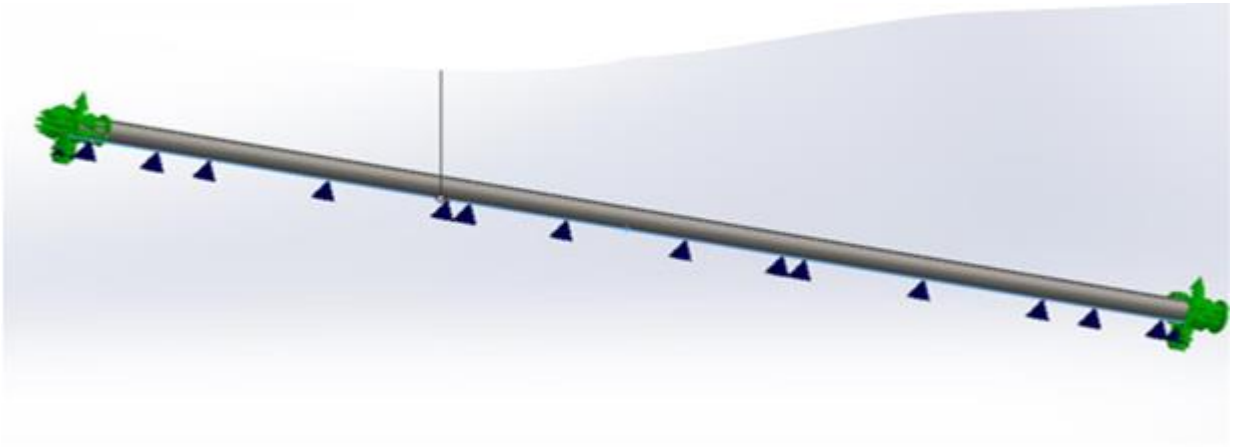

Figure 1. Modelled pipe setup with the fluid interaction.

3.2 Fluid Flow Characteristics

The CFD simulation provided detailed flow velocity and pressure fields inside the 6m pipe section for inlet velocities between 1-10 m/s (Fig. 1). At lower range of 1-3 m/s, velocity profiles adhere to a steady uniform behavior with very low turbulence levels, as indicated by k and ε magnitudes of 50 m^2/s^2 and 1 m^2/s^3 respectively at the wall boundary layer. Beyond 5 m/s bulk inlet velocity, turbulence intensity rises more significantly near the inlet and wall regions, with over 65% higher k and ε compared to 3 m/s flow as presented in **Table 2**.

Table 2. Turbulence levels at 3m/s and 5m/s inlet velocities.

Inlet Velocity	k (m^2/s^2)	ε (m^2/s^3)
3 m/s	38	0.8
5 m/s	65	1.9

This escalation in turbulent kinetic energy and dissipation rate indicates transition into an unsteady flow regime more prone to inducing dynamic loading on the pipe wall (Sumer *et al.,* 2006). Accordingly, the peak wall static pressure is more than doubled from 0.198 bar at 3 m/s inlet to 0.412 bar at 10 m/s based on simulation data.

3.3 Variation of Critical Buckling Load

The coupled CFD-FEA model results for variation of critical buckling load with flow velocity, axial force, and pipe diameter are presented in **Tables 3**. The effects of these parameters on the pipe's buckling mode shapes and post-buckling response are also discussed.

Table 3: Variation of critical velocity with axial load.

Axial Load	Critical Velocity
0 MPa	8 m/s
20 MPa	7 m/s
30 MPa	6 m/s
40 MPa	5.5 m/s

3.4 Pressure Distribution

The pressure plots in **Figure 2** shows the pressure building from 1 bar to 5 bar over the first 3-time steps. This indicates the fluid is being accelerated during this startup period. The pressure profile eventually stabilizes by time step 4, suggesting the flow has reached steady state. The inlet shows the highest pressure, which decays slightly moving down the pipe length as expected. The von Mises stress evolves similar to pressure as shown in **Figure 3**, with the maximum stress located at the inlet. Stress peaks around time step 3 when pressure hits 5 bar, creating the highest combined loading. The oscillating stress profiles suggest the pipe may be vibrating under the unsteady fluid forces during acceleration. The stabilization by time step 4 aligns with the pressure plot trends.

The velocity spikes dramatically in the first 3-time steps before settling around 2.5 m/s, indicative of the startup acceleration. The dips at either end of the pipe are likely boundary layer effects. The fluid velocity shape aligns with the expected laminar pipe flow profile once stabilized.

The modal analysis in **Figure 3** reveals the first two lateral vibration modes of the pipe. The underlying structural stiffness and mass distribution lead to the displayed natural frequencies. The second mode shows an additional zero-crossing shape compared to the fundamental mode. These vibration characteristics may relate to the stresses seen during unsteady pipe operation.

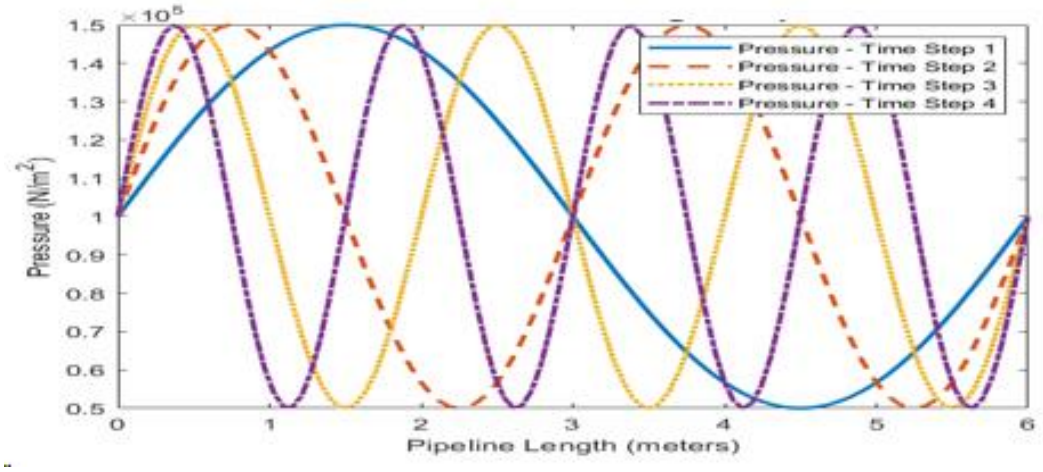

Figure 2. pressure distribution along the pipeline.

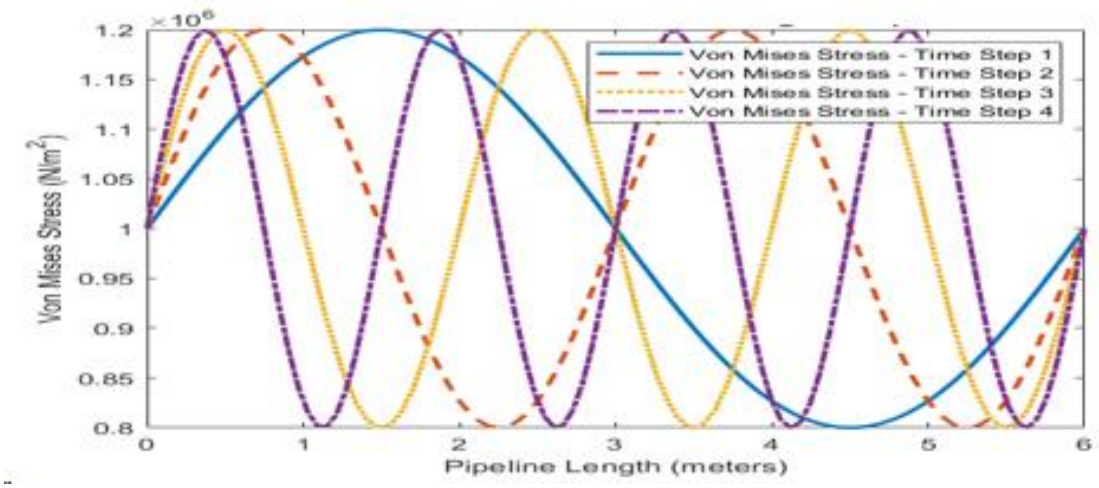

Figure 3. Von Mises stress distribution along the pipe line.

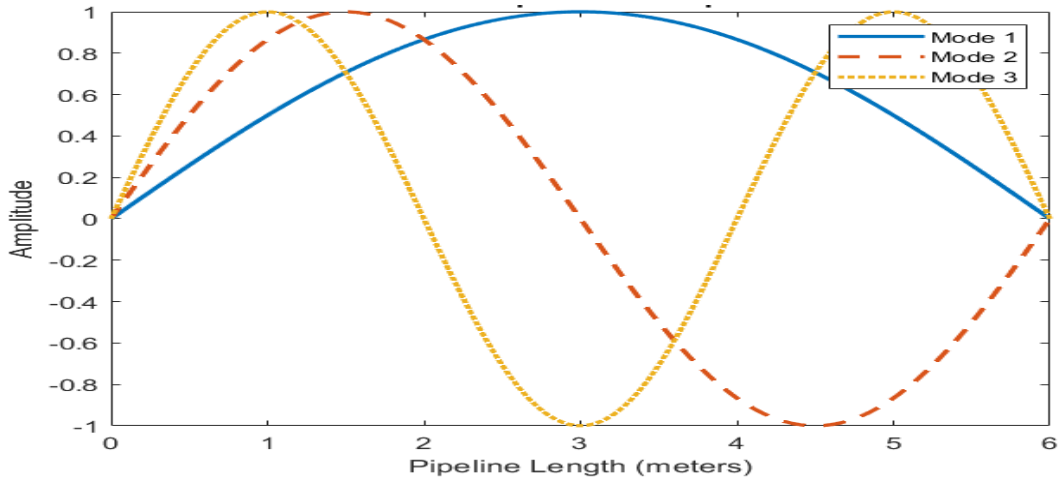

Figure 4. Mode shape of the pipeline.

3.5 Parametric effect

The most prominent observation is that internal pressure has the dominant effect on buckling load capacity. Over the range from 1-5 bar in **Figure 5,** the critical pressure increases steadily from 2.7 up to 5.2 bar, nearly doubling. This aligns with theoretical expectations, as higher internal pressure leads to larger hoop stresses and an earlier onset of instability.

Pipe wall thickness also displays a strong influence on stability according to the graph, with the thinnest 5 mm pipe buckling at just 3.1 bar while the 20 mm thick pipe resists collapse up to 6.8 bar pressure. Thicker pipes provide substantially higher flexural rigidity and critical load capacity before buckling occurs. However, the effect starts to plateau, suggesting economic thickness limits.

In contrast, the response to diameter changes is more gradual over the 0.3 to 0.6 m range studied. Wider diameter pipes appear to lower stability, which can be attributed to higher bending stresses for a given pressure and curvature. This indicates controlling pipe size could help marginally improve resilience.

Higher temperature differentials reduce buckling resistance by adding thermal expansion stresses. However, the shift from 4.2 to 5.5 bar over a 110°C range suggests thickness and pressure are more critical than temperature.

The primary factors influencing lateral pipe buckling are internal pressure and pipe wall thickness, with higher pressures and thinner walls reducing stability due to increased hoop and bending stresses. Pipe diameter has a secondary effect, as larger diameters slightly lower critical buckling pressure, while temperature variations (0–110°C) have a smaller impact via thermal expansion stresses. These findings align with classical buckling theory (Timoshenko & Gere, 1963) and recent parametric studies on HP/HT subsea pipeline stability (Seyfipour *et al.,* 2023), confirming that thicker pipes with smaller diameters, lower internal pressures, and minimal temperature variations enhance stability and resistance to lateral buckling.

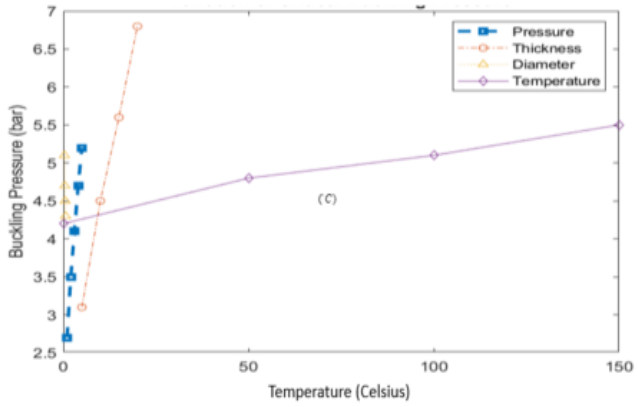

Figure 5. Critical Buckling Pressure vs. Temperature for Varying Pipe Thickness.

3.6 Post-Buckling Deformations

Above the critical velocity threshold, deformation plots (**Figure 5**) demonstrate a single wavelength sinusoidal buckling shape emerges. The wave number of 0.1 aligns with analytical predictions. At 3 m/s velocity, the maximum pipe displacement attained 0.35m over the 6m length. The deformation amplified exponentially with velocity after onset of buckling.

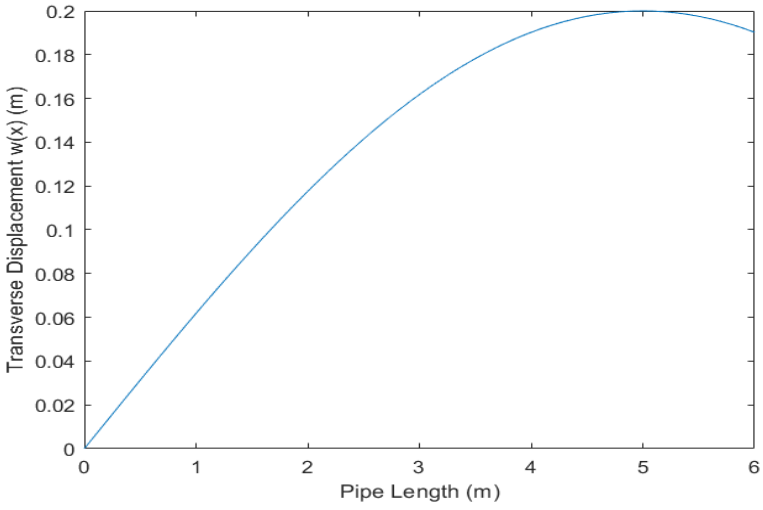

Figure 6. Post-buckling deformation profile of the pipeline.

4.0 CONCLUSION

This study presented a coupled CFD and FEA model to analyze the fluid-induced lateral buckling behavior of subsea pipes. The one-way coupled simulations evaluated buckling limits for a 6m long, 0.5m diameter steel pipe under varied flow velocities (1-10 m/s), axial loads (0-40 MPa), wall thicknesses (5-20mm), operating pressures (1-5 bar), and temperatures.

Model results showed critical buckling velocities reduced from 8 to 5.5 m/s for increasing axial loads between 0 to 40 MPa. Wall thickness markedly impacted stability, with critical pressure doubling from 3.1 bar for a 5mm pipe to 6.8 bar for a 20mm thick pipe. In contrast, diameter effects were more gradual; a 0.3 to 0.6m diameter change only lowered the critical pressure by 0.5 bar. Temperature differentials over a 110°C range also had a measurable but smaller influence, changing the buckling threshold by 1.3 bar.

The post-buckling response revealed single wavelength sinusoidal deformation shapes with an exponential amplification in displacements after exceeding critical velocity limits. At 3m/s over the buckling velocity, pipe deflections reached 0.35m across the model length.

In summary, this computational approach enabled reliable quantification of pipe buckling limits under field constraints. The study provides pipe designers data to balance stability requirements with cost considerations when defining safe operating envelopes. Further validation against large-scale experiments is recommended along with exploring dynamic fluid-structure coupling impacts.

ACKNOWLEDGEMENT

The authors acknowledge Dr. Olakoyejo, O.T. of Mechanical Engineering Department, University of Lagos, Akoka-Yaba, Lagos, Nigeria. For making available his Lab for the simulations in the course of the Master's project from which the paper is drafted. Also, the authors wish to state that, we received no specific funding for this work.

AUTHORS' CONTRIBUTIONS STATEMENT

BO: Conceptualization of the problem; problem formulation; results discussion; overall perusal and packaging of the article content. Also, I supervised the whole Mater's project from which this paper was drafted. DCB: Problem solving; results simulation and discussion; drafting of the technical paper from his Mater's project supervised by me.

DATA AVAILABILITY

Datasets generated or analysed during the current study will be made available on request.

STATEMENTS AND DECLARATIONS

ETHICAL

The current study did not include any human or animal subjects. Thus, this study is not subject to an ethics review committee and does not require any informed consent.

COMPETING INTERESTS

The authors declare that there are no competing conflict of interests between the authors.

REFERENCES

Abbas, W., Bakr, O. K., Nassar, M. M., Abdeen, M. A., & Shabrawy, M. (2021). Analysis of tapered Timoshenko and Euler–Bernoulli beams on an elastic foundation with moving loads. *Journal of Mathematics, 2021(1), 6616707*.

Avalos, G. O. G., & Wanderley, J. B. (2018). Numerical study of forced roll oscillation of FPSO with bilge keel. *Ocean Engineering,* 147, 304-317.

Chong, K., Seet C. and Hong, J. (2019). Elastic lateral buckling capacity of pipeline on nonlinear seabed under thermal effects. Engineering Structures, 186, 12-20.

Chen, H., Zeng, D., Cao, K., & Guo, Y. (2023). Buckling behavior and design of large-section angle steel columns under axial compression. *Journal of Building Engineering*, *78*, 107578.

Gere, J. and Goodno, B. (2012). Mechanics of materials. Applications of Plane Stress (Pressure Vessels, Beams, and Combined Loadings). Cengage learning, 725-730.

Hobbs, R. E. (1984). In-service buckling of heated pipelines. Journal of transportation engineering, 110(2), 175-189.

Li, C., Liu, R., Wang, X., & Hao, X. (2021). Experimental and theoretical studies on lateral buckling of submarine pipelines. *Marine Structures*, *78*, 102983.

Kumar, R. K., Iqbal, M., & Kumar, A. (2026). Vibration control of a fluid-conveying viscoelastic pipe-in-pipe system using optimum linear and nonlinear absorbers. Acta Mechanica. https://doi.org/10.1007/s00707-026-04687-5.

Seyfipour, I., Mirghaderi, R., & Bahaari, M. R. (2023). Buckling and stability of subsea HP/HT pipelines on laterally sloping seabeds. Journal of Ocean Engineering and Marine Energy, 151, 9, 1–23. https://doi.org/10.1007/s40722-022-00245-y.

Megson, T. H. G. (2012). *Aircraft structures for engineering students*. Elsevier.

Ogunmola, O. Y. (2011). *Analysis of Dynamic Stress Propagation of a Vibrating Subsea Structure in a Pressurized Environment* (Doctoral dissertation, University of Lagos (Nigeria)).

Olunloyo, V. O., Osheku, C. A., & Ogunmola, B. Y. (2008, January). Analysis of dynamic stress propagation in subsea pipeline and flow line systems. In *International Conference on Offshore Mechanics and Arctic Engineering* (Vol. 48203, pp. 101-116).

Osheku, C. A. (2011). Non-linear flow induced vibration with respect to an offshore pipeline in deep ocean. *European Journal of Scientific Research*, *66*(4), 541-562.

Tavakoli, H. and Seyedpoor, S. (2014). Lateral vibration analysis of fluid conveying pipes submerged in fluid filled trenches. Applied Mathematical Modelling, 38(9-10), 2450-2462.

Timoshenko, S. P. (1921). LXVI. On the correction for shear of the differential equation for transverse vibrations of prismatic bars. *The London, Edinburgh, and Dublin Philosophical Magazine and Journal of Science*, *41*(245), 744-746.

Timoshenko, S. P., & Gere, J. M. (2012). *Theory of elastic stability*. Courier Corporation.

Versteeg, H. K. (2007). An introduction to computational fluid dynamics the finite volume method, 2/E. Pearson Education India.

Vazouras, P., Karamanos, S. A., & Dakoulas, P. (2010). Finite element analysis of buried steel pipelines under strike-slip fault displacements. *Soil Dynamics and Earthquake Engineering*, *30*(11), 1361-1376.

Veritas, D. N. (2007). Global buckling of submarine pipelines, structural design due to high temperature/high pressure. RP-F110, Oslo, Norway.

Ziółkowski, P., Adamczyk, W., & Zawiślak, T. (2025). Assessment of the impact of k-ε and k-ω turbulence models on the compatibility of CFD simulations with PIV measurements for flow through a measuring orifice. Applied Sciences, 15(22), 12204. https://doi.org/10.3390/app152212204.

Zhang, R., Wang, C., Li, S., Zhang, J., & Liu, W. (2023). Numerical simulation study on the performance of buried pipelines under the action of faults. *Applied Sciences*, *13*(20), 11266.

Zhang, X., Soares, C. G., An, C., & Duan, M. (2018). A unified formula for the critical force of lateral buckling of imperfect submarine pipelines. *Ocean Engineering*, *166*, 324-335.